NANO LETTERS

pubs.acs.org/NanoLett Letter

Giant and Tunable Out-of-Plane Spin Polarization of Topological Antimonene

Polina M. Sheverdyaeva,*,∞ Conor Hogan,*,∞ Gustav Bihlmayer, Jun Fujii, Ivana Vobornik, Matteo Jugovac, Asish K. Kundu, Sandra Gardonio, Zipporah Rini Benher, Giovanni Di Santo, Sara Gonzalez, Luca Petaccia, Carlo Carbone, and Paolo Moras

Cite This: *Nano Lett.* 2023, 23, 6277−6283 Read Online

ACCESS | Metrics & More | Article Recommendations | Supporting Information

ABSTRACT: Topological insulators are bulk insulators with metallic and fully spin-polarized surface states displaying Dirac-like band dispersion. Due to spin-momentum locking, these topological surface states (TSSs) have a predominant in-plane spin polarization in the bulk fundamental gap. Here, we show by spin-resolved photoemission spectroscopy that the TSS of a topological insulator interfaced with an antimonene bilayer exhibits nearly full out-of-plane spin polarization within the substrate gap. We connect this phenomenon to a symmetry-protected band crossing of the spin-polarized surface states. The nearly full out-of-plane spin polarization of the TSS occurs along a continuous path in the energy−momentum space, and the spin polarization within the gap can be reversibly tuned from nearly full out-of-plane to nearly full in-plane by electron doping. These findings pave the way to advanced spintronics applications that exploit the giant out-of-plane spin polarization of TSSs.

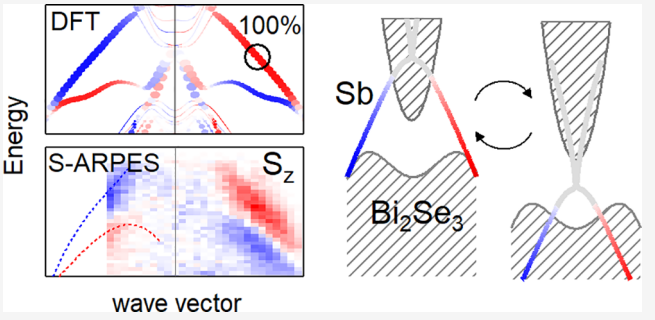

KEYWORDS: *density functional theory, spin-resolved ARPES, electronic structure, topological insulators, 2D materials, antimonene*

Topological insulators (TIs) are a class of materials with high spin−orbit coupling (SOC) and nontrivial band topology.[1] They are insulating in the bulk and metallic at the surfaces due to the presence of robust Dirac-like topological surface states (TSSs) protected by time-reversal symmetry. TSSs are fully spin-polarized with a predominantly in-plane spin orientation near the Fermi level (E_F) as dictated by the symmetry of the spin-momentum locking. The charge−spin interconversion effects arising from this spin texture have remarkable applications in spintronics.[2] For example, the injection of an electric current into a TI is known to generate in-plane spin-transfer torques (STTs) orders of magnitude larger than in other materials with high SOC.[3] These giant STTs are suitable for low-power current-induced magnetization switching in TI/ferromagnetic layer heterostructures.[3]

A new spectrum of spintronic effects and related applications would open up if TIs with out-of-plane surface spin texture could be designed.[4,5] In the context of current-induced magnetization switching, out-of-plane STTs are expected to be more efficient than in-plane STTs in reversing the magnetization of layers with perpendicular magnetic anisotropy, which are typically used in logic and memory devices.[6] Nonetheless, to date, only a few TSSs have shown significant out-of-plane spin polarization. Record values above 20% have been experimentally reported for Bi_2Te_3,[7] Sb_2Te_3,[8] $PbBi_2Te_4$,[9] and BiTeI,[10] yet they remain much lower than the corresponding in-plane spin components. For this reason, phenomena associated with the out-of-plane spin polarization of the TSSs are still poorly explored experimentally.[4,11]

The spin texture of a prototypical TI, Bi_2Se_3, was reported to be strongly modified upon the formation of an interface with a bilayer (BL) of honeycomb-like (β-) antimonene.[12] The topological proximity effect leads to a hybrid TSS that is confined within the antimonene BL and the topmost Se layer (hereon, TSS_{Sb}). A reversal of the in-plane spin texture and a significant out-of-plane spin polarization were noted in density functional theory (DFT) calculations.[12] Here, we provide for the first time a clear experimental demonstration of the phenomenon by means of spin- and angle-resolved photoemission spectroscopy (spin-ARPES) and provide a quantitative, microscopic analysis of its origin using DFT. We show that the out-of-plane spin polarization of TSS_{Sb} reaches giant values of up to 94% within the substrate gap. We connect its emergence to a protected band crossing of fully polarized

Received: January 12, 2023
Revised: July 8, 2023
Published: July 17, 2023

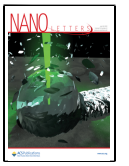

https://doi.org/10.1021/acs.nanolett.3c00153
Nano Lett. 2023, 23, 6277−6283

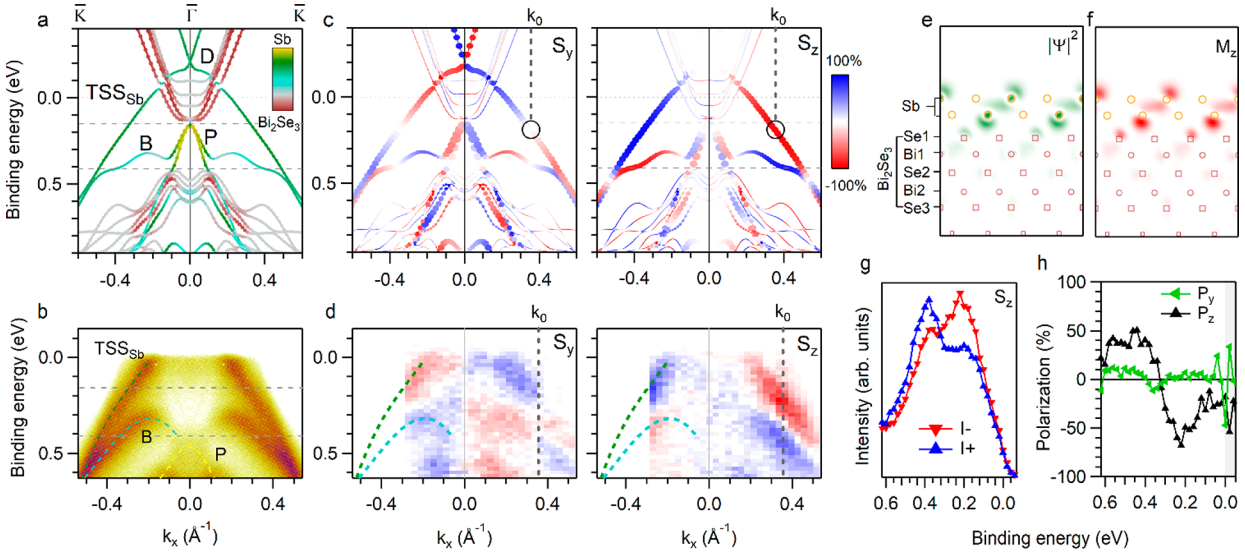

Figure 1. Theoretical and experimental electronic structure of antimonene/Bi_2Se_3 along the $\overline{K\Gamma K}$ direction. (a) Band structure calculations. The color scale indicates the localization of the states. (b) ARPES data taken at $h\nu$ = 14 eV. (c) Calculated in-plane (left) and out-of-plane (right) spin components. The size of the data points indicates the projection onto the Sb atoms. (d) Experimental in-plane (left) and out-of-plane (right) spin- and angle-resolved photoemission intensities measured with $h\nu$ = 16 eV. (e) Charge density profile and (f) out-of-plane magnetization distribution of TSS_{Sb} (through the plane intersecting the Sb−Sb bond and topmost Se atom) at the position marked by a circle in panel (c). (g) Out-of-plane spin-resolved photoemission spectra taken at k_0. (h) Spin polarization spectra for the in-plane and out-of-plane spin components at k_0.

surface states along $\overline{\Gamma M}$. Similar band crossings of surface states were recently reported as two-dimensional analogs of tilted Weyl cones.[13,14] Importantly, the nearly full out-of-plane spin polarization of TSS_{Sb} is not limited to a certain direction but occurs among a wide range of wave vectors. We demonstrate that the degree of out-of-plane spin polarization of TSS_{Sb} inside the Bi_2Se_3 gap can be finely and reversibly tuned by the adsorption of alkali metals or carbon oxide. We propose that similar spin textures may occur in other systems of heterostructures comprising TIs and that such interfaces can be seen as a viable way to tailor the out-of-plane spin texture of TIs.

We recall the electronic structure of the heterostructure formed by one BL of antimonene (i.e., one layer of strongly buckled honeycomb-like β-antimonene[15]) and the Bi_2Se_3 substrate.[12,16,17] Figure 1(a) shows the calculated band structure along the $\overline{K\Gamma K}$ direction (k_x axis). The color scale indicates the spatial localization of the electronic states. Three bands are located within the fundamental gap of the substrate (gray dashed lines indicate the gap edges):[18] P is localized in antimonene, TSS_{Sb} in antimonene and the topmost Se layer (Figure 1(e), by close analogy to the case of Bi-terminated Bi_2Te_3[19]), and B at the interface. TSS_{Sb} can be seen as the migration of the TSS of the substrate (TSS_{BS}) to the antimonene BL upon formation of the heterostructure (topologization of antimonene by the proximity effect).[12,16,20] The Dirac point D lies 0.2 eV above E_F in a local gap of the Bi_2Se_3 conduction band. The three aforementioned bands can be identified in the ARPES spectra of Figure 1(b) ($h\nu$ = 14 eV). At this photon energy, the Bi_2Se_3-related spectral features are strongly suppressed, thus allowing for better visibility of antimonene-derived states. (See for comparison ref 12 and Figure S1(a).) TSS_{Sb} and B (green and light-blue dashed lines) are in good agreement with the DFT calculations (see also Figure S2(a,b) and ref 12), while P (yellow dashed line) lies at higher binding energies than expected (Figure S2(c,d)). The gray dashed lines indicate the experimental position of the Bi_2Se_3 fundamental gap in the antimonene/Bi_2Se_3 heterostructure (Figure S1(a)). TSS_{Sb} crosses the entire gap, and only the top part of B enters the gap. P lies below the bottom of the gap, where it overlaps and hybridizes with the Bi_2Se_3 states. Thus, the electronic structure and spin structure of the system within the fundamental gap of Bi_2Se_3 are determined by TSS_{Sb} and B, on which we focus from here onward.

Figure 1(c) shows the calculated in-plane (S_y) and out-of-plane (S_z) spin components for the electronic states of antimonene/Bi_2Se_3. TSS_{Sb} is fully in-plane spin-polarized near D, by close analogy to the behavior of TSS_{BS}.[21] Its S_y component decreases steeply below D and reverses at k_0 = 0.35 Å^{-1} (black circle at 0.19 eV), in agreement with the literature.[12,16] We quantitatively analyzed the S_z component of TSS_{Sb} at k_0 and observed a surprisingly high value of close to 94%. It remains larger than S_y throughout the fundamental gap of Bi_2Se_3 and reaches about 57% at E_F. B shows a similar predominance of S_z over S_y and an opposite spin texture with respect to TSS_{Sb}.

The spin-ARPES data of Figure 1(d) confirm the predicted properties of TSS_{Sb} and B. The in-plane spin textures of TSS_{Sb} and B are reversed at k_0. At this point, the out-of-plane spin polarization P_z is about 66% for TSS_{Sb} and 48% for B, and the in-plane ones are close to zero (Figure 1(g,h) and Figure S3(a)). These as-measured out-of-plane spin polarizations are about twice as large as the so far experimentally reported values for the TSSs, despite being lower, as typically observed, than theoretically predicted due to extrinsic and intrinsic effects.[7,8,11] While referring to the total spin polarization $P_{tot} = \sqrt{P_x^2 + P_y^2 + P_z^2}$,[8,11] the P_z values at k_0 reach 99 and 98% for TSS_{Sb} and B, respectively, in very good agreement with the values predicted by DFT. The complete inversion of S_y and S_z textures at opposite k_x values (Figure 1(d)) and the agreement with the DFT calculations show that the present measurements capture the spin polarization of TSS_{Sb} and B in the initial state,[11,22] which is the relevant property for

https://doi.org/10.1021/acs.nanolett.3c00153
Nano Lett. 2023, 23, 6277−6283

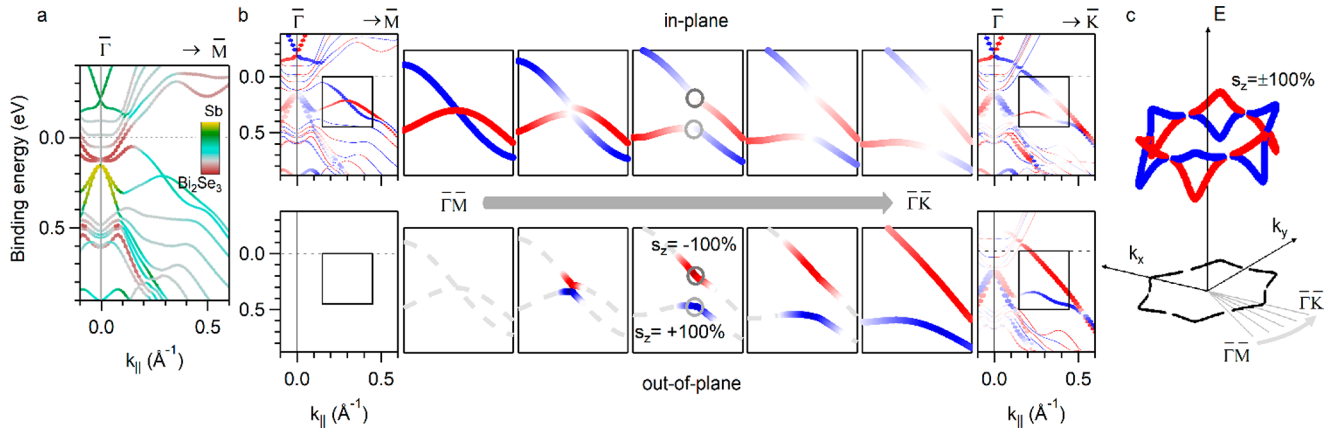

Figure 2. Origin of the giant out-of-plane spin texture. (a) Band structure calculations along $\overline{\Gamma M}$. The color scale indicates the localization of the states. (b) Spin-resolved band structure. Top row: in-plane spin component of the TSS_{Sb} and B bands along radial axes comprised between $\overline{\Gamma M}$ and $\overline{\Gamma K}$. Bottom row: same as the top row for the out-of-plane spin component. Along $\overline{\Gamma M}$, the computed S_z is zero. Gray circles mark the states with zero in-plane and ±100% out-of-plane spin components in the central panels. Band dispersions away from high-symmetry directions are shown schematically. (c) Schematic representation of the S_z = ±100% contours for TSS_{Sb} and B in the energy−momentum space.

spintronics. As expected from symmetry considerations, P_z is zero along $\overline{M\Gamma M}$ (Figure S3(b)).

The spin texture of TSS_{Sb} within the Bi_2Se_3 fundamental gap differs remarkably from that of other TSSs in the absolute size of the (giant) S_z values and in the predominance of S_z over S_y. For example, the predicted and measured S_z values for the TSSs of Bi_2Te_3[7,8] and $PbBi_2Te_4$[9] are 30−40% and about 20%, respectively. In Bi_2Te_3, the out-of-plane spin component is very small at E_F, increases moving away from the Dirac point, and reaches its maximum above E_F.[7] In the case of antimonene/Bi_2Se_3, instead, S_z of TSS_{Sb} is giant within the substrate's gap and remains predominant between E_F and 0.5 eV. So far, giant S_z values have been reported only for the states of transition-metal dichalcogenides[23,24] or Bi films,[25] which lack topological protection.[26] Another important difference with respect to these materials concerns the spatial properties of TSS_{Sb} where S_z is maximal (circle in Figure 1(c)). Here, TSS_{Sb} displays a high surface localization (Figure 1(e)) and a uniform orientation of the magnetization pattern (Figure 1(f)), whereas the magnetization pattern in WSe_2 and Bi_2Te_3 switches from positive to negative moving from one atomic plane to the next.[7,24,27] This high surface spin localization and absence of the spin reversal may lead to large spin decoherence times, which are appealing for spintronic applications.[7,28]

In order to explore the origin of the unusually high S_z values of TSS_{Sb} and B, we followed the evolution of their spin texture by artificially increasing the distance between antimonene and Bi_2Se_3 (Figure S4). The calculated S_z is weak in both nearly free-standing antimonene and Bi_2Se_3; therefore, the observed giant S_z is an exclusive property of the heterostructure. In contrast to WSe_2, where states with dominant d_z^2/p_z character exhibit strongly suppressed S_z,[24] the charge density profile has a dominant p_z component[16] that hardly changes as a function of distance (Figure S5). According to ref 29, the presence of an in-plane electric field can also give rise to a high S_z. We analyzed different stacking arrangements of antimonene and Bi_2Se_3 atomic layers (Figure S6) and found that the out-of-plane spin texture is reversed only when the *substrate* stacking—and thus the local potential gradient—is modified. However, since the out-of-plane electric field is normally much larger than the in-plane one, these results would not explain the unusually high, almost fully out-of-plane spin polarization.

In Figure 2, we demonstrate that the giant S_z values of TSS_{Sb} and B are derived from the constraint imposed by mirror symmetry on their in-plane spin texture. Figure 2(a) shows the band structure of the heterostructure along the $\overline{\Gamma M}$ direction. We can observe TSS_{Sb} and B bands that cross close to the 0.25 eV binding energy. The top (bottom) row of Figure 2(b) shows the in-plane (out-of-plane) spin components of TSS_{Sb} and B along radial axes comprised between $\overline{\Gamma M}$ and $\overline{\Gamma K}$. Since the spin projection along the wave vector direction is forbidden by the symmetry of the Rashba model,[30] the sum of the spin components shown in the top and bottom rows is always 100% for every state. In particular, along $\overline{\Gamma M}$ both states are fully in-plane spin-polarized. Similar band crossings of fully polarized surface states were recently reported experimentally and referred to as two-dimensional analogs of tilted Weyl cones.[13,14] The mirror symmetry along $\overline{\Gamma M}$ protects their accidental crossing from opening a gap. Moving away from $\overline{\Gamma M}$ toward $\overline{\Gamma K}$, the symmetry constraint vanishes and a gap can open (Figure S7). Since the spin texture of the bands far from the gap region is maintained, the in-plane spin component is forced to become zero while approaching the gap (top row). This results in the emergence of nearly full out-of-plane spin components with opposite signs for TSS_{Sb} and B (bottom row). We emphasize that TSS_{Sb} and B display giant S_z not only along $\overline{\Gamma K}$ but everywhere in the momentum space, except along the six $\overline{\Gamma M}$ axes. This is qualitatively different from the S_z of TSSs of TIs related to their hexagonal warping, that reaches its maximum along $\overline{\Gamma K}$. The points where S_z is maximal, i.e., close to 100% (two gray circles mark these points in the central panels of Figure 2(b), as an example), form the two wavy contours displayed in Figure 2(c). Importantly, they are fully located within the bulk band gap of the substrate.

We now explore the possibility of tuning the out-of-plane spin texture of antimonene/Bi_2Se_3 via electron doping. Figure 3(a) shows the band structure of the system with a 0.25 monolayer (ML) of K on top of antimonene in the most stable atomic configuration. (Section 2 in the Supporting Information, Figures S8−S10, and Table S1 consider other structures and coverages.) Here, 1 ML corresponds to the density of the uppermost Sb plane. The K-induced electron doping influences the antimonene- and Bi_2Se_3-related features differ-

https://doi.org/10.1021/acs.nanolett.3c00153
Nano Lett. 2023, 23, 6277−6283

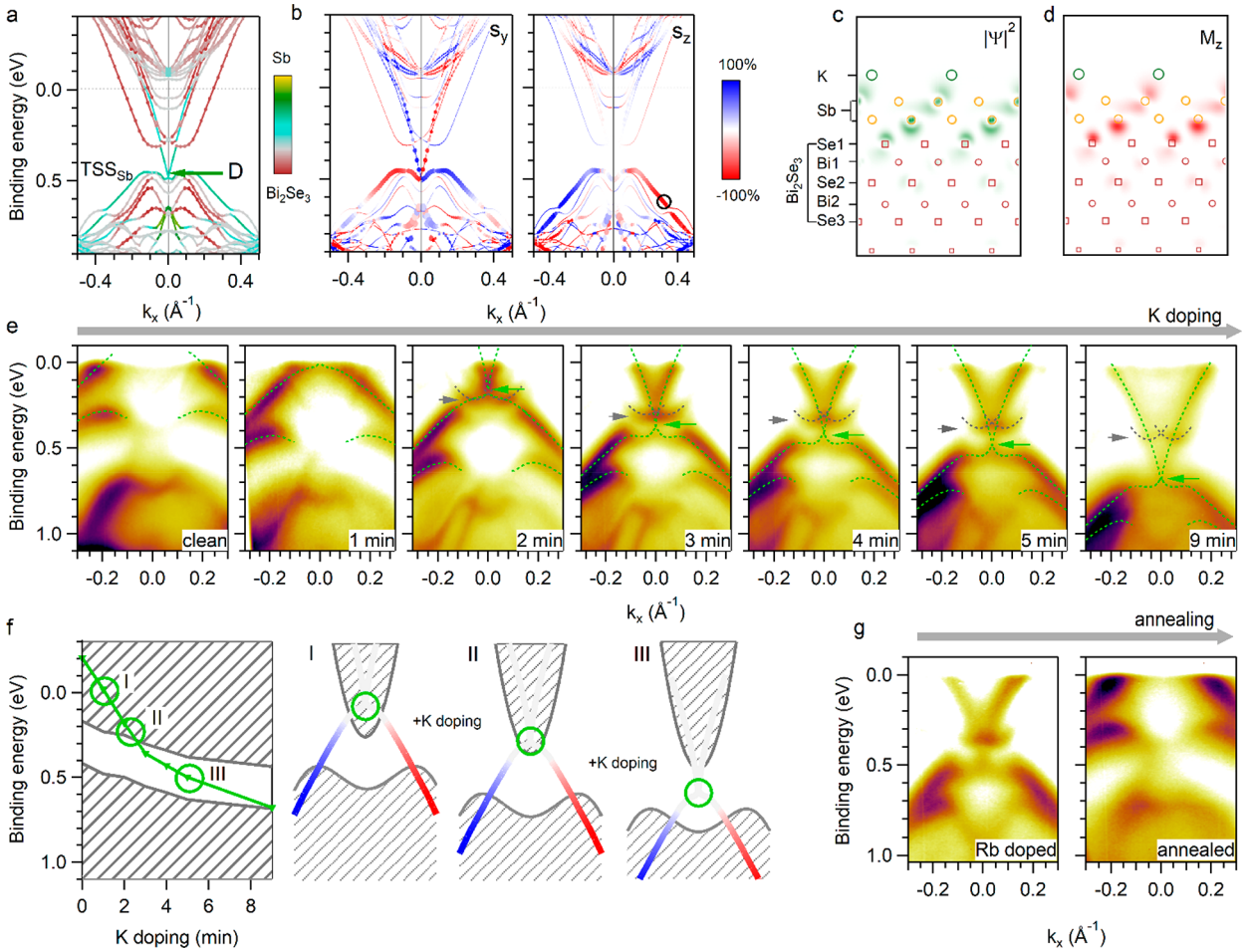

Figure 3. Tailoring of the spin texture by electron doping. (a) Band structure calculations for 0.25 ML K/antimonene/Bi_2Se_3. The color scale indicates the localization of the states. (b) Calculated in-plane (left) and out-of-plane (right) spin components. The size of the data points indicates the projection onto the Sb atoms. (c) Charge density profile and (d) out-of-plane magnetization distribution of TSS_{Sb} at the position marked by a circle in panel (b). (e) ARPES spectra along $\overline{K\Gamma K}$ as a function of the K coverage, $h\nu$ = 14 eV. (f) Position of D (green) with respect to the bulk band edges (gray) and the schematics of the out-of-plane spin texture of TSS_{Sb} as a function of the K deposition. (g) ARPES spectra of antimonene/Bi_2Se_3 doped by Rb before and after annealing to 350 K.

ently due to the presence of a surface dipole (Figure S11). D is shifted toward higher binding energy by 0.7 eV (green arrow at 0.5 eV below E_F) and toward the bulk Bi_2Se_3 bands by only 0.3 eV. This relative energy shift strongly alters the spin texture of the system (Figure 3(b)). Now TSS_{Sb} shows pronounced S_y and negligible S_z components within the entire fundamental gap of Bi_2Se_3. (B becomes degenerate with the bulk valence states of the Bi_2Se_3.) This behavior is expected on the basis of the spin structure of TSS_{Sb} above D (Figure 1(c)) and the analogous relative shift between TSS_{BS} and the bulk bands observed upon alkali metal deposition on Bi_2Se_3.[31−33] Notably, TSS_{Sb} retains the strongly localized character (Figure 3(c)) and the constant out-of-plane magnetization pattern (Figure 3(d)) of the pristine antimonene/Bi_2Se_3 system.

The electronic structure shown in Figure 3(a) is actually observed by ARPES when K is deposited on the surface of antimonene/Bi_2Se_3 (Figure 3(e)). As the amount of K increases, TSS_{Sb} and B (green dashed lines) continuously shift toward higher binding energies. D (green arrow) becomes visible from 2 min deposition and reaches 0.7 eV at saturation coverage. Starting from the 2 min deposition, we also observe two inverted parabolas (gray dashed lines) that shift toward higher binding energy as the K doping increases (Figure S1(b−d)). By comparison with the calculations of Figure 3(a) and the ARPES data of K-doped Bi_2Se_3,[31] these bands can be identified with the bottom of the bulk conduction band of Bi_2Se_3. Since the size of the fundamental gap of Bi_2Se_3 is known (0.25 eV), it is possible to locate D with respect to the bulk band edges at each K deposition step, as shown on the left side of Figure 3(f). The resulting electronic structure of the system, regarding TSS_{Sb} only, is schematically shown on the right side of Figure 3(f). In pristine or lightly K-doped antimonene/Bi_2Se_3 (I), the spin texture in the fundamental gap of Bi_2Se_3 is dominated by states with giant S_z. With increasing K coverage, the S_z component of TSS_{Sb} decreases (II) and eventually disappears (III).

A similar electron doping effect can be induced by dosing Rb or CO on antimonene/Bi_2Se_3 held at liquid nitrogen temperature (left side of Figure 3(g) and Figure S12). Also in this case, we observe the downward shift of TSS_{Sb} and B and the appearance of two inverted parabolas, by close analogy to the K-doped system. Similar to Bi_2Se_3,[31] the effect of K, Rb, and CO dosing can be removed by raising the temperature of the antimonene/Bi_2Se_3 system, thus making the electron doping effect largely reversible (right side of Figure 3(g) and Figure S12) and repeatable (Figure S13).

https://doi.org/10.1021/acs.nanolett.3c00153
Nano Lett. 2023, 23, 6277−6283

Our analysis demonstrates that it is possible to design topological systems with giant S_z components by interfacing existing TIs with trivial materials, such as semiconducting antimonene. The antimonene/Bi_2Se_3 heterostructure features a single spin channel inside the bulk gap with a giant out-of-plane spin polarization and topological protection, which is strongly localized in the surface. This system satisfies an important requirement for spintronic applications, i.e., the tunability of spin- and electronic properties.[34−37] The out-of-plane spin polarization can indeed be finely and reversibly tuned from almost 100% to 0%. This final state can also be reached via absorption of other elements, such as Mg and Ca.[38] The simple band structure described above can be used as a model for the simulation and experimental testing of transport properties for spintronic devices and could be implemented in magnetic memory applications.

The mechanism described above, in which a fully out-of-plane spin polarization arises from a symmetry-protected Weyl-like band crossing, to the best of our knowledge has not been reported in the literature. We suggest that it may manifest in other systems that feature protected band crossing along a line of mirror symmetry. In the context of topologically protected states, a band crossing along the $\overline{\Gamma M}$ direction and exhibiting a similar in-plane spin texture reversal was observed in the related system of double BL antimonene on Bi_2Se_3.[12] A protected band crossing followed by a nearly full S_z may well exist also in similar heterostructures that manifest a topological proximity effect, i.e., antimonene on Bi_2Te_3, Sb_2Te_3, and Bi_2Se_2Te.[16,39,40] A crossing of spin-polarized surface bands along a high-symmetry line was experimentally reported for NbGeSb[13] and W(110).[14] Although these states lack topological protection, one may also expect full out-of-plane spin polarization away from mirror symmetry planes in these systems.

METHODS

High-quality single crystals of Bi_2Se_3 were grown by the Bridgman method. Bismuth and selenium were purchased from Sigma-Aldrich at 99.999% and ≥99.5% trace metal basis, respectively. The stoichiometric amounts of high-purity elements were sealed in evacuated quartz ampules and heated to 1023 at 21 K/h. The ampules were maintained at that temperature for 48 h. Thereafter, the temperature was slowly reduced to 523 K at 5 K/h and then cooled to room temperature.

Sb was deposited on freshly cleaved Bi_2Se_3 at room temperature and subsequently annealed to 430 K to form the β-antimonene phase as described in refs 12, 17, and 41. Potassium and rubidium were deposited on the sample kept at 80 K at a rate of 0.04 monolayer (ML)/min (as referenced to the density of the Bi_2Se_3 surface). CO adsorption was achieved by cooling the sample from room temperature to 80 K in a CO atmosphere. The LEED pattern showed sharp 1 × 1 spots at all preparation stages (Figure S14).

DFT calculations were performed within a plane-wave/pseudopotential framework as implemented in the quantum-ESPRESSO (QE) code.[42] Spin−orbit coupling was incorporated via use of fully relativistic ultrasoft pseudopotentials[43,44] with a kinetic energy cutoff of 45 Ry. The Bi_2Se_3 surface was modeled by using a centrosymmetric slab containing six quintuple layers. The four topmost atomic layers (plus the antimonene layer and the K atoms) were allowed to relax during structural optimization. The experimental lattice constant of 4.143 Å was used.[45] The PBE functional[46] and Grimme-D2 van der Waals correction[47] were adopted. This computational scheme yielded results in close agreement with our previous studies using QE and VASP.[12,17] The equilibrium distance d_0 = 2.32 Å and the 1 × 1 lattice matching considered in the calculations are justified in previous structural studies of the system.[12,20] Adsorption of potassium was simulated using 1 × 1, 2 × 2, and 3 × 3 supercells, corresponding to coverages of 1, 0.25, and 0.11 ML. Several on-top and intercalated geometries were investigated, as shown in Section 2 of the Supporting Information.

The ARPES experiments were carried out at the APE-LE,[48] BaDElPh,[49] and VUV-photoemission beamlines of the synchrotron Elettra (Trieste, Italy) with $h\nu$ = 14−60 eV and p-polarized light, while keeping the sample at 80 K. The electron spectrometers were placed at an angle between 42° and 50°, with reference to the direction of the incoming p-polarized photon beam. The energy resolution was about 20 meV, and the momentum resolution was about 0.02 $Å^{-1}$. Spin-resolved ARPES data were taken at the APE-LE beamline by using a Scienta-Omicron DA30 hemispherical analyzer operating in deflection mode and equipped with two orthogonal VLEED reflectometers, with an energy resolution of about 90 meV and a momentum resolution of about 0.04 $Å^{-1}$. During the spin measurements, the analyzer's slits were set parallel to the $\overline{K\Gamma K}$ direction, and the spin-ARPES spectra along high-symmetry directions were obtained by using the deflectors without moving the sample. The spin polarization was calculated as described in ref 48 and using the Sherman function value S = 0.26.

ASSOCIATED CONTENT

Data Availability Statement

The data that support the findings of this study are available within the article and Supporting Information. Extra data are available from the corresponding authors upon reasonable request.

Supporting Information

The Supporting Information is available free of charge at https://pubs.acs.org/doi/10.1021/acs.nanolett.3c00153.

Additional experimental data (ARPES and spin-ARPES data, LEED patterns) as well as DFT calculations useful to understanding the theoretical results shown in the main text (PDF)

AUTHOR INFORMATION

Corresponding Authors

Polina M. Sheverdyaeva − *Istituto di Struttura della Materia-CNR (ISM-CNR), 34149 Trieste, Italy;* orcid.org/0000-0002-4231-1638; Email: polina.sheverdyaeva@ism.cnr.it

Conor Hogan − *Istituto di Struttura della Materia-CNR (ISM-CNR), 00133 Roma, Italy; Dipartimento di Fisica, Università di Roma "Tor Vergata", 00133 Roma, Italy;* orcid.org/0000-0002-0870-6361; Email: conor.hogan@ism.cnr.it

Authors

Gustav Bihlmayer − *Peter Grünberg Institut and Institute for Advanced Simulation, Forschungszentrum Jülich and JARA, D-52425 Jülich, Germany;* orcid.org/0000-0002-6615-1122

https://doi.org/10.1021/acs.nanolett.3c00153
Nano Lett. 2023, 23, 6277−6283

Jun Fujii − *Istituto Officina dei Materiali (IOM)-CNR, Laboratorio TASC, 34149 Trieste, Italy*
Ivana Vobornik − *Istituto Officina dei Materiali (IOM)-CNR, Laboratorio TASC, 34149 Trieste, Italy;* orcid.org/0000-0001-9957-3535
Matteo Jugovac − *Istituto di Struttura della Materia-CNR (ISM-CNR), 34149 Trieste, Italy; Peter Grünberg Institut PGI, Forschungszentrum Jülich, 52425 Jülich, Germany;* Present Address: (M.J.): Elettra - Sincrotrone Trieste S.C.p.A., Strada Statale 14 km 163.5, 34149 Trieste, Italy.; orcid.org/0000-0001-9525-3980
Asish K. Kundu − *Istituto di Struttura della Materia-CNR (ISM-CNR), 34149 Trieste, Italy; International Center for Theoretical Physics (ICTP), Trieste 34151, Italy;* Present Address: (A.K.K.): Condensed Matter Physics and Materials Science Division, Brookhaven National Laboratory, Upton, New York 11973, United States.; orcid.org/0000-0003-2199-1053
Sandra Gardonio − *Materials Research Laboratory, University of Nova Gorica, Ajdovščina 5270, Slovenia;* orcid.org/0000-0002-5560-718X
Zipporah Rini Benher − *Materials Research Laboratory, University of Nova Gorica, Ajdovščina 5270, Slovenia;* orcid.org/0000-0003-3923-750X
Giovanni Di Santo − *Elettra - Sincrotrone Trieste S.C.p.A., 34149 Trieste, Italy;* orcid.org/0000-0001-9394-2563
Sara Gonzalez − *Elettra - Sincrotrone Trieste S.C.p.A., 34149 Trieste, Italy;* Present Address: (S.G.): Institut des Nanotechnologies de Lyon, UMR5270, 69621 Villeurbanne, France
Luca Petaccia − *Elettra - Sincrotrone Trieste S.C.p.A., 34149 Trieste, Italy;* orcid.org/0000-0001-8698-1468
Carlo Carbone − *Istituto di Struttura della Materia-CNR (ISM-CNR), 34149 Trieste, Italy*
Paolo Moras − *Istituto di Struttura della Materia-CNR (ISM-CNR), 34149 Trieste, Italy;* orcid.org/0000-0002-7771-8737

Complete contact information is available at: https://pubs.acs.org/10.1021/acs.nanolett.3c00153

Author Contributions

[∞]P.M.S. and C.H. contributed equally to this work

Notes

The authors declare no competing financial interest.

■ ACKNOWLEDGMENTS

We acknowledge EUROFEL-ROADMAP ESFRI of the Italian Ministry of Education, University, and Research. A.K.K. acknowledges receipt of a fellowship from the ICTP-TRIL Programme, Trieste, Italy. We acknowledge Elettra Sincrotrone Trieste for providing access to its synchrotron radiation facilities. This work has been partly performed in the framework of the nanoscience foundry and fine analysis (NFFA-MUR Italy Progetti Internazionali) facility. C.H. acknowledges CINECA under the ISCRA initiative for the availability of high-performance computing resources and support. S. Gardonio and Z. Rini Benher gratefully acknowledge financial support from the Slovenian Research Agency (Research Core Funding No. P2-0412).

■ REFERENCES

(1) Zhang, H.; Liu, C.-X.; Qi, X.-L.; Dai, X.; Fang, Z.; Zhang, S.-C. Topological insulators in Bi2Se3, Bi2Te3 and Sb2Te3 with a single Dirac cone on the surface. *Nat. Phys.* **2009**, *5*, 438−442.
(2) Zhang, S.; Fert, A. Conversion between spin and charge currents with topological insulators. *Phys. Rev. B* **2016**, *94*, 184423.
(3) Mellnik, A. R.; Lee, J. S.; Richardella, A.; Grab, J. L.; Mintun, P. J.; Fischer, M. H.; Vaezi, A.; Manchon, A.; Kim, E.-A.; Samarth, N.; Ralph, D. C. Spin-transfer torque generated by a topological insulator. *Nature* **2014**, *511*, 449−451.
(4) Han, J.; Liu, L. Topological insulators for efficient spin-orbit torques. *APL Materials* **2021**, *9*, 060901.
(5) Liu, Y.; Shao, Q. Two-Dimensional Materials for Energy-Efficient Spin-Orbit Torque Devices. *ACS Nano* **2020**, *14* (8), 9389−9407.
(6) Ikeda, S.; Miura, K.; Yamamoto, H.; Mizunuma, K.; Gan, H. D.; Endo, M.; Kanai, S.; Hayakawa, J.; Matsukura, F.; Ohno, H. A perpendicular-anisotropy CoFeB-MgO magnetic tunnel junction. *Nat. Mater.* **2010**, *9*, 721−724.
(7) Herdt, A.; Plucinski, L.; Bihlmayer, G.; Mussler, G.; Döring, S.; Krumrain, J.; Grützmacher, D.; Blügel, S.; Schneider, C. M. Spin-polarization limit in Bi2Te3 Dirac cone studied by angle- and spin-resolved photoemission experiments and ab initio calculations. *Phys. Rev. B* **2013**, *87*, 035127.
(8) Nomura, M.; Souma, S.; Takayama, A.; Sato, T.; Takahashi, T.; Eto, K.; Segawa, K.; Ando, Y. Relationship between Fermi surface warping and out-of-plane spin polarization in topological insulators: A view from spin- and angle-resolved photoemission. *Phys. Rev. B* **2014**, *89*, 045134.
(9) Eremeev, S. V.; Landolt, G.; Menshchikova, T. V.; Slomski, B.; Koroteev, Y. M.; Aliev, Z. S.; Babanly, M. B.; Henk, J.; Ernst, A.; Patthey, L.; et al. Atom-specific spin mapping and buried topological states in a homologous series of topological insulators. *Nat. Commun.* **2012**, *3*, 635.
(10) Sakano, M.; Bahramy, M. S.; Katayama, A.; Shimojima, T.; Murakawa, H.; Kaneko, Y.; Malaeb, W.; Shin, S.; Ono, K.; Kumigashira, H.; et al. Strongly Spin-Orbit Coupled Two-Dimensional Electron Gas Emerging near the Surface of Polar Semiconductors. *Phys. Rev. Lett.* **2013**, *110*, 107204.
(11) Dil, J. Hugo. Spin- and angle-resolved photoemission on topological materials. *Electron. Struct.* **2019**, *1*, 023001.
(12) Holtgrewe, K.; Mahatha, S. K.; Sheverdyaeva, P. M.; Moras, P.; Flammini, R.; Colonna, S.; Ronci, F.; Papagno, M.; Barla, A.; Petaccia, L.; et al. Topologization of β-antimonene on Bi2Se3 via proximity effects. *Sci. Rep.* **2020**, *10*, 14619.
(13) Marković, I.; Hooley, C. A.; Clark, O. J.; Mazzola, F.; Watson, M. D.; Riley, J. M.; Volckaert, K.; Underwood, K.; Dyer, M. S.; Murgatroyd, P. A. E.; et al. Weyl-like points from band inversions of spin-polarised surface states in NbGeSb. *Nat. Commun.* **2019**, *10*, 5485.
(14) Varykhalov, A.; Marchenko, D.; Sánchez-Barriga, J.; Golias, E.; Rader, O.; Bihlmayer, G. Tilted Dirac cone on W(110) protected by mirror symmetry. *Phys. Rev. B* **2017**, *95*, 245421.
(15) Aktürk, O. Ü.; Özçelik, V. O.; Ciraci, S. Single-layer crystalline phases of antimony: Antimonenes. *Phys. Rev. B* **2015**, *91*, 235446.
(16) Jin, K.-H.; Yeom, H. W.; Jhi, S.-H. Band structure engineering of topological insulator heterojunctions. *Phys. Rev. B* **2016**, *93*, 075308.
(17) Flammini, R.; Colonna, S.; Hogan, C.; Mahatha, S. K.; Papagno, M.; Barla, A.; Sheverdyaeva, P. M.; Moras, P.; Aliev, Z. S.; Babanly, M. B.; et al. Evidence of β-antimonene at the Sb/Bi2Se3 interface. *Nanotechnology* **2018**, *29*, 065704.
(18) Nechaev, I. A.; Hatch, R. C.; Bianchi, M.; Guan, D.; Friedrich, C.; Aguilera, I.; Mi, J. L.; Iversen, B. B.; Blügel, S.; Hofmann, P.; Chulkov, E. V. Evidence for a direct band gap in the topological insulator Bi2Se3 from theory and experiment. *Phys. Rev. B* **2013**, *87*, 121111.
(19) Hirahara, T.; Bihlmayer, G.; Sakamoto, Y.; Yamada, M.; Miyazaki, H.; Kimura, S.-I.; Blügel, S.; Hasegawa, S. Interfacing 2D

and 3D Topological Insulators: Bi(111) Bilayer on Bi2Te3. *Phys. Rev. Lett.* **2011**, *107*, 166801.
(20) Holtgrewe, K.; Hogan, C.; Sanna, S. Evolution of Topological Surface States Following Sb Layer Adsorption on Bi2Se3. *Materials* **2021**, *14*, 1763.
(21) Hsieh, D.; Xia, Y.; Qian, D.; Wray, L.; Dil, J. H.; Meier, F.; Osterwalder, J.; Patthey, L.; Checkelsky, J. G.; Ong, N. P.; et al. A tunable topological insulator in the spin helical Dirac transport regime. *Nature* **2009**, *460*, 1101.
(22) Bigi, C.; Mazzola, F.; Fujii, J.; Vobornik, I.; Panaccione, G.; Rossi, G. Measuring spin-polarized electronic states of quantum materials: 2H-NbSe2. *Phys. Rev. B* **2021**, *103*, 245142.
(23) Bawden, L.; Cooil, S. P.; Mazzola, F.; Riley, J. M.; Collins-Mcintyre, L. J.; Sunko, V.; Hunvik, K. W. B.; Leandersson, M.; Polley, C. M.; Balasubramanian, T.; et al. Spin-valley locking in the normal state of a transition-metal dichalcogenide superconductor. *Nat. Commun.* **2016**, *7*, 11711.
(24) Riley, J. M.; Mazzola, F.; Dendzik, M.; Michiardi, M.; Takayama, T.; Bawden, L.; Granerød, C.; Leandersson, M.; Balasubramanian, T.; Hoesch, M.; et al. Direct observation of spin-polarised bulk bands in an inversion-symmetric semiconductor. *Nat. Phys.* **2014**, *10*, 835−839.
(25) Takayama, A.; Sato, T.; Souma, S.; Takahashi, T. Giant Out-of-Plane Spin Component and the Asymmetry of Spin Polarization in Surface Rashba States of Bismuth Thin Film. *Phys. Rev. Lett.* **2011**, *106*, 166401.
(26) Aguilera, I.; Kim, H.-J.; Friedrich, C.; Bihlmayer, G.; Blügel, S. Z2 topology of bismuth. *Phys. Rev. Mater.* **2021**, *5*, L091201.
(27) Henk, J.; Ernst, A.; Eremeev, S. V.; Chulkov, E. V.; Maznichenko, I. V.; Mertig, I. Complex Spin Texture in the Pure and Mn-Doped Topological Insulator Bi2Te3. *Phys. Rev. Lett.* **2012**, *108*, 206801.
(28) Schliemann, J. Colloquium: Persistent spin textures in semiconductor nanostructures. *Rev. Mod. Phys.* **2017**, *89*, 011001.
(29) Friedrich, R.; Caciuc, V.; Bihlmayer, G.; Atodiresei, N.; Blügel, S. Designing the Rashba spin texture by adsorption of inorganic molecules. *New J. Phys.* **2017**, *19*, 043017.
(30) Bychkov, Y. A.; Rashba, É. I. Properties of a 2D electron gas with lifted spectral degeneracy. *JETP Lett.* **1984**, *39*, 78.
(31) Zhu, Z.-H.; Levy, G.; Ludbrook, B.; Veenstra, C. N.; Rosen, J. A.; Comin, R.; Wong, D.; Dosanjh, P.; Ubaldini, A.; Syers, P.; et al. Rashba Spin-Splitting Control at the Surface of the Topological Insulator Bi_2Se_3. *Phys. Rev. Lett.* **2011**, *107*, 186405.
(32) Bianchi, M.; Hatch, R. C.; Mi, J.; Iversen, B. B.; Hofmann, P. Simultaneous quantization of bulk conduction and valence states through adsorption of nonmagnetic impurities on Bi_2Se_3. *Phys. Rev. Lett.* **2011**, *107*, 086802.
(33) Förster, T.; Krüger, P.; Rohlfing, M. Ab initio studies of adatom- and vacancy-induced band bending in Bi_2Se_3. *Phys. Rev. B* **2015**, *91*, 035313.
(34) Kondou, K.; Yoshimi, R.; Tsukazaki, A.; Fukuma, Y.; Matsuno, J.; Takahashi, K. S.; Kawasaki, M.; Tokura, Y.; Otani, Y. Fermi-level-dependent charge-to-spin current conversion by Dirac surface states of topological insulators. *Nat. Phys.* **2016**, *12*, 1027−1031.
(35) Su, S. H.; Chuang, P.-Y.; Chen, H.-Y.; Weng, S.-C.; Chen, W.-C.; Tsuei, K.-D.; Lee, C.-K.; Yu, S.-H.; Chou, M.M.-C.; Tu, L.-W.; et al. Topological Proximity-Induced Dirac Fermion in Two-Dimensional Antimonene. *ACS Nano* **2021**, *15*, 15085−15095.
(36) Sun, R.; Yang, S.; Yang, X.; Vetter, E.; Sun, D.; Li, N.; Su, L.; Li, Y.; Li, Y.; Gong, Z.-Z.; Xie, Z.-K.; Hou, K.-Y.; Gul, Q.; He, W.; Zhang, X.-Q.; Cheng, Z.-H. Large Tunable Spin-to-Charge Conversion Induced by Hybrid Rashba and Dirac Surface States in Topological Insulator Heterostructures. *Nano Lett.* **2019**, *19*, 4420−4426.
(37) Barfuss, A.; Dudy, L.; Scholz, M. R.; Roth, H.; Höpfner, P.; Blumenstein, C.; Landolt, G.; Dil, J. H.; Plumb, N. C.; Radovic, M.; et al. Elemental Topological Insulator with Tunable Fermi Level: Strained α-Sn on InSb(001). *Phys. Rev. Lett.* **2013**, *111*, 157205.
(38) Upadhyay, S.; Srivastava, P. DFT study of adsorption and diffusion of Mg, K, Ca over monolayer antimonene. *IOP Conf. Ser.: Mater. Sci. Eng.* **2021**, *1120*, 012035.
(39) Lei, T.; Liu, C.; Zhao, J.-L.; Li, J.-M.; Li, Y.-P.; Wang, J.-O.; Wu, R.; Qian, H.-J.; Wang, H.-Q.; Ibrahim, K. Electronic structure of antimonene grown on Sb_2Te_3 (111) and Bi_2Te_3 substrates. *J. Appl. Phys.* **2016**, *119*, 015302.
(40) Lei, T.; Li, J.-M.; Lu, S.; Wang, L.; Yu, Q.; Li, F.-S.; Wang, J.-O.; Wang, H.-Q.; Ibrahim, K.; Zhang, K. Electronic states driven by the crystal field in two-dimensional materials: The case of antimonene. *Phys. Rev. B* **2022**, *105*, 115404.
(41) Hogan, C.; Holtgrewe, K.; Ronci, F.; Colonna, S.; Sanna, S.; Moras, P.; Sheverdyaeva, P. M.; Mahatha, S.; Papagno, M.; Aliev, Z. S.; Babanly, M.; Chulkov, E. V.; Carbone, C.; Flammini, R. Temperature Driven Phase Transition at the Antimonene/Bi2Se3 van der Waals Heterostructure. *ACS Nano* **2019**, *13*, 10481−10489.
(42) Giannozzi, P.; Baroni, S.; Bonini, N.; Calandra, M.; Car, R.; Cavazzoni, C.; Ceresoli, D.; Chiarotti, G. L.; Cococcioni, M.; Dabo, I.; et al. QUANTUM ESPRESSO: a modular and open-source software project for quantum simulations of materials. *J. Phys.: Condens. Matter* **2009**, *21*, 395502.
(43) Dal Corso, A.; Mosca Conte, A. Spin-orbit coupling with ultrasoft pseudopotentials: Application to Au and Pt. *Phys. Rev. B* **2005**, *71*, 115106.
(44) Dal Corso, A. Pseudopotentials periodic table: From H to Pu. *Comput. Mater. Sci.* **2014**, *95*, 337.
(45) Nakajima, S. The crystal structure of $Bi_2Te_{3-x}Se_x$. *J. Phys. Chem. Solids* **1963**, *24*, 479.
(46) Perdew, J. P.; Burke, K.; Ernzerhof, M. Generalized Gradient Approximation Made Simple. *Phys. Rev. Lett.* **1996**, *77*, 3865.
(47) Grimme, S. J. Semiempirical GGA-type density functional constructed with a long-range dispersion correction. *Comput. Chem.* **2006**, *27*, 1787.
(48) Bigi, C.; Das, P. K.; Benedetti, D.; Salvador, F.; Krizmancic, D.; Sergo, R.; Martin, A.; Panaccione, G.; Rossi, G.; Fujii, J.; Vobornik, I. Very efficient spin polarization analysis (VESPA): new exchange scattering-based setup for spin-resolved ARPES at APE-NFFA beamline at Elettra. *J. Synchrotron Radiat.* **2017**, *24*, 750.
(49) Petaccia, L.; Vilmercati, P.; Gorovikov, S.; Barnaba, M.; Bianco, A.; Cocco, D.; Masciovecchio, C.; Goldoni, A. BaD ElPh: A 4 m normal-incidence monochromator beamline at Elettra. *Nucl. Inst. Meth. Phys. Res. A* **2009**, *606*, 780.

https://doi.org/10.1021/acs.nanolett.3c00153
Nano Lett. 2023, 23, 6277−6283